

## Article

# Comparative Analysis of Secondary Organic Aerosol Formation during PM<sub>2.5</sub> Pollution and Complex Pollution of PM<sub>2.5</sub> and O<sub>3</sub> in Chengdu, China

Tianli Song <sup>1</sup>, Miao Feng <sup>2</sup> , Danlin Song <sup>2</sup>, Song Liu <sup>1</sup>, Qinwen Tan <sup>2</sup>, Yuancheng Wang <sup>2</sup>, Yina Luo <sup>2</sup>, Xi Chen <sup>2,\*</sup> and Fumo Yang <sup>1</sup>

<sup>1</sup> College of Architecture and Environment, Sichuan University, Chengdu 610065, China

<sup>2</sup> Chengdu Academy of Environmental Sciences, Chengdu 610072, China

\* Correspondence: chenx@cdaes.org.cn

**Abstract:** Nowadays, many cities in China are suffering from both fine particulate matter (PM<sub>2.5</sub>, particulate matter with an aerodynamic diameter smaller than 2.5 μm) and ozone (O<sub>3</sub>) pollution. Secondary organic aerosol (SOA) is an important component of PM<sub>2.5</sub> and is closely related to the oxidation processes. To investigate the characteristics and formation pathways of SOA during different types of haze pollution episodes, carbonaceous components of PM<sub>2.5</sub> and volatile organic compounds (VOCs) were monitored continuously in Chengdu in April 2019, when Chengdu experienced not only PM<sub>2.5</sub> pollution (SPP) but also a complex pollution of PM<sub>2.5</sub> and O<sub>3</sub> (CoP). In the CoP episode, the concentrations of SOA increased by 51.2% as compared to SPP, and the SOA concentrations were positively correlated with PM<sub>2.5</sub> mass concentrations. These suggest that SOA drove the increase in PM<sub>2.5</sub> levels during the haze event to some extent. The preliminary VOC source analysis based on the feature ratio showed that vehicle emission and fuel volatilization sources were the main sources of VOCs at this urban site. In addition, coal emissions and biomass burning were also important contributors. High-carbon alkanes and aromatic hydrocarbons significantly contributed to the SOA formation. These results provide a preliminary understanding of SOA formation during different types of pollution episodes in Chengdu, which can help us to further understand air pollution in this typical region.

**Keywords:** Chengdu; PM<sub>2.5</sub> pollution; complex pollution of PM<sub>2.5</sub> and O<sub>3</sub>; secondary organic aerosol; VOCs



**Citation:** Song, T.; Feng, M.; Song, D.; Liu, S.; Tan, Q.; Wang, Y.; Luo, Y.; Chen, X.; Yang, F. Comparative Analysis of Secondary Organic Aerosol Formation during PM<sub>2.5</sub> Pollution and Complex Pollution of PM<sub>2.5</sub> and O<sub>3</sub> in Chengdu, China. *Atmosphere* **2022**, *13*, 1834. <https://doi.org/10.3390/atmos13111834>

Academic Editor: Jo-Chun Kim

Received: 1 October 2022

Accepted: 2 November 2022

Published: 4 November 2022

**Publisher's Note:** MDPI stays neutral with regard to jurisdictional claims in published maps and institutional affiliations.



**Copyright:** © 2022 by the authors. Licensee MDPI, Basel, Switzerland. This article is an open access article distributed under the terms and conditions of the Creative Commons Attribution (CC BY) license (<https://creativecommons.org/licenses/by/4.0/>).

## 1. Introduction

Surface ozone (O<sub>3</sub>) and fine particulate matter (PM<sub>2.5</sub>, particulate matter with an aerodynamic diameter smaller than 2.5 μm) are major air pollutants in China [1,2]. Since the implementation of the Action Plan for Air pollution Prevention and Control (2013–2017) [3] and the Three-Year Action Plan to Win the Battle for Blue Sky (2018–2020) [4], PM<sub>2.5</sub> concentration has decreased significantly across the nation [5]. However, current PM<sub>2.5</sub> concentrations still regularly exceed the national air quality standard, and O<sub>3</sub> pollution is becoming more and more severe [6]. Although high PM<sub>2.5</sub> concentrations tend to occur in the cold seasons, and O<sub>3</sub> pollution is more frequent in the warm seasons [1,7], there are days when PM<sub>2.5</sub> and O<sub>3</sub> pollution occur simultaneously, which is often referred to as the complex pollution of PM<sub>2.5</sub> and O<sub>3</sub> (CoP) [8–10].

Secondary organic aerosol (SOA) is a major component of PM<sub>2.5</sub>, which is generated through homogeneous and heterogeneous reactions of volatile organic compounds (VOCs) and intermediate/semi-VOCs as well as the aging of primary aerosols in the ambient atmosphere [11,12]. Meanwhile, the formation of O<sub>3</sub> is closely related to VOCs and NO<sub>x</sub>. In other words, VOCs are one of the important precursors of secondary PM<sub>2.5</sub> and O<sub>3</sub> [13].

On the one hand, it can generate atmospheric oxidizing species such as  $O_3$  through photochemical reactions, thereby promoting the generation of secondary inorganic and organic components of  $PM_{2.5}$ ; on the other hand, it can also be directly converted into secondary organic components of  $PM_{2.5}$  [14,15]. Previous studies on SOA have typically involved the measurement of carbonaceous components [16,17] and SOA tracers [18,19] in PM as well as its gaseous precursors, VOCs [12,20].

The Sichuan Basin (SCB) is one of the most polluted areas in China [21]. Influenced by intense anthropogenic activities and frequent stagnant conditions as well as its complex basin topography, the SCB has suffered from severe  $PM_{2.5}$  and  $O_3$  pollution [7]. As the capital city of the SCB, Chengdu is a highly urbanized megacity, and its air pollution characteristics have attracted a lot of attention. In 2021, Chengdu was identified as one of the first cities in China to carry out the tracking study of “One City, One Policy” for the coordinated prevention and control of  $PM_{2.5}$  and  $O_3$  (<https://www.mee.gov.cn/>, accessed on 15 October 2022). However, as far as we know, previous air pollution studies on Chengdu mainly focused on single PM pollution [22–25] and single  $O_3$  pollution [26–29] as well as on the long-term characteristics of pollutants [30–33]. These studies also focused on the observation of individual  $PM_{2.5}$  components or individual VOC components. Only Song et al. [34] analyzed the formation mechanism of extreme haze events in Chengdu by simultaneously measuring  $PM_{2.5}$  components and VOCs. Furthermore, to our knowledge, few studies have characterized pollutants in CoP in Chengdu, which crucially limits our ability to coordinate the prevention and control of  $PM_{2.5}$  and  $O_3$  in this region.

In this study, we conducted a comprehensive online observation of the carbonaceous components of  $PM_{2.5}$  and VOCs in urban Chengdu from 1 April to 30 April 2019, during which a CoP episode occurred immediately after a  $PM_{2.5}$  pollution (SPP) episode. The purpose of this study was to perform a comparative analysis of these two types of pollution episodes, which mainly included investigating the amount of SOA generation and the characteristics of VOCs during the different episodes.

## 2. Materials and Methods

### 2.1. Sampling Site

The sampling site was located on the rooftop of the Chengdu Academy of Environmental Sciences in Qingyang District ( $30.65^\circ$  N,  $104.04^\circ$  E, approximately 25 m above the ground). As shown in Figure 1, the site is located within the 2nd ring elevated road of Chengdu, surrounded by a mix of commercial and residential areas as well as dense traffic emissions, which make it a typical urban site in Chengdu [25,34].

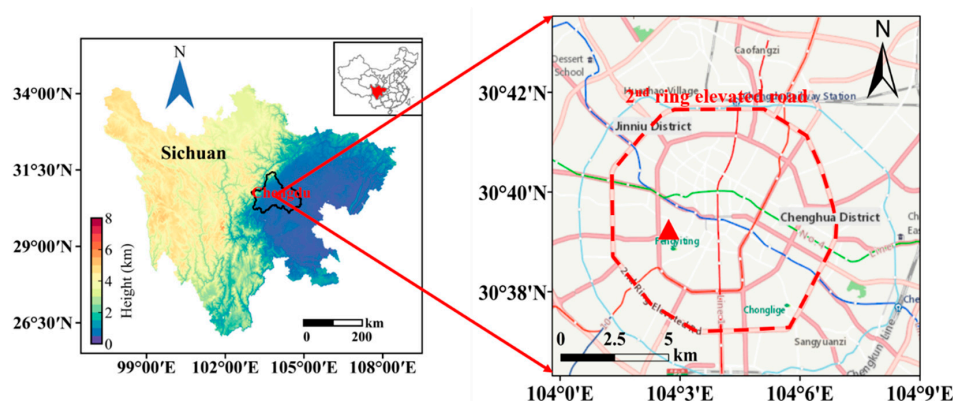


**Figure 1.** The location of the sampling site in urban areas of Chengdu.

### 2.2. Instruments

In this campaign, online monitoring instruments were used to obtain hourly resolution observations. All instrumental analyses were subject to regular laboratory quality control and quality assurance (QC/QA), including the strict enforcement of daily calibration

and daily monitoring, which are detailed in a previous study [35]. PM<sub>2.5</sub> concentrations were monitored by a tapered element oscillating microbalance instrument (TEOM 1405-F, Thermo Fisher, Waltham, MA, USA). Organic carbon (OC) and elemental carbon (EC) in PM<sub>2.5</sub> were detected by a semi-continuous OC/EC analyzer (Type 4, Sunset Laboratories, Hicksville, NY, USA). Fifty-six VOC species were continuously monitored by a gas chromatograph (GC955-611/811, Synspec Corporation, Groningen, The Netherlands) with dual detectors, including a flame ionization detector (FID, for C2-C5 hydrocarbon measurements) and a dual photoionization detector (PID, for C6-C12 hydrocarbon measurements). Gaseous pollutants (NO<sub>2</sub>, NO, CO, and O<sub>3</sub>) were detected by a series of gas analyzers (17i/17i/48i/49i, Thermo Fisher, USA). In addition, a micro weather station instrument (WS600-UMB, Lufft, Fellbach, Germany) was used to measure the meteorological parameters, including temperature (T), relative humidity (RH), wind speed (WS), wind direction (WD), and precipitation (PP).

### 2.3. Data Analysis

#### 2.3.1. Estimation of SOA in PM<sub>2.5</sub>

The minimum OC/EC ratio method has been widely used to estimate the concentration of SOC in particulate matters, which is calculated as shown below [36]:

$$\text{POC} = \left( \frac{\text{OC}}{\text{EC}} \right)_{\text{pri}} \times \text{EC} \quad (1)$$

$$\text{SOC} = \text{OC} - \left( \frac{\text{OC}}{\text{EC}} \right)_{\text{pri}} \times \text{EC} \quad (2)$$

$$\text{POA} = 1.5 \times \text{SOC} \quad (3)$$

$$\text{SOA} = 2.3 \times \text{SOC} \quad (4)$$

where OC and EC are the measured concentrations of OC and EC in PM<sub>2.5</sub>, respectively; primary OC (POC) and SOC are the estimated primary and secondary organic carbon concentrations, respectively. The primary OA (POA) and SOA were calculated by multiplying the corresponding OC by the ratios of 1.5 and 2.3, respectively, which were obtained from online aerosol mass spectrometry observations conducted in the SCB [37]. From the above equation, it is clear that the critical step in estimating POC and SOC is the determination of an appropriate primary OC/EC ratio. In this study, the minimum R squared (MRS) method with a clear quantitative criterion was used to estimate the appropriate (OC/EC)<sub>pri</sub> value [16]. As shown in Figure S1, the actual (OC/EC)<sub>pri</sub> corresponding to the minimum R<sup>2</sup> (SOC vs. EC) is 3.1.

#### 2.3.2. Estimation of SOA Generation from VOCs

The atmospheric oxidation process of VOCs by OH radical, NO<sub>3</sub> radical, and O<sub>3</sub> was an important pathway for SOA generation [38]. To investigate the relationship between SOA and VOCs, we calculated the amount of SOA produced through the photochemical oxidation of VOCs based on the measured SOA yield in the smog chamber and the estimated VOC consumption [12,39]. The detailed calculation formula is as follows [12]:

$$\text{SOA}_i = \text{VOC}_{i,\text{consumed}} \times Y_i \quad (5)$$

where the VOC<sub>i,consumed</sub> is the consumption of *i*th VOC species; Y<sub>*i*</sub> is the SOA yield from the oxidation of the *i*th VOC species, determined by chamber studies. Previous studies have reported zero SOA yields for small alkanes and alkenes, low yields for higher (>C8) alkanes and cycloalkanes, and the highest SOA yields for aromatics [38]. In our study, the SOA yields for alkanes were taken from the study by Lim and Ziemann [40], and those for aromatics were recalculated by Wang et al. [12] based on a previous chamber study [39]. The vapor wall losses in the chamber studies were recognized to have been

largely underestimated [12], and thus all the yields were also corrected by the vapor loss biases from Zhang et al. [41]. The SOA yields used in this study are tabulated in Table S1.

The photochemical consumption of VOCs can be calculated by Equation (7) below, with the assumption that the oxidation of OH radicals dominates the loss of VOCs in the ambient atmosphere.

$$\text{VOC}_{i,\text{consumed}} = \text{VOC}_{i,t} \times (\exp(-k_i[\text{OH}]\Delta t) - 1) \quad (6)$$

where  $\text{VOC}_{i,t}$  and  $\text{VOC}_{i,\text{consumed}}$  are the measured and consumed concentration of the  $i$ th VOC species, respectively;  $k_i$  is the rate constant of the  $i$ th VOC species with OH radicals,  $\text{cm}^3/\text{molecule}/\text{s}$ ;  $[\text{OH}]$  and  $\Delta t$  are the OH radical concentrations and the determined photochemical age, respectively, and their product is the OH exposure.

The OH exposure is derived from the photochemical age, usually by selecting two VOC species of the same origin but with very different  $k_{\text{OH}}$  values [42–44]. In this study, *m*, *p*-xylenes (X) and ethylbenzene (E) were selected to calculate the ambient OH exposure [43,45]. Hence, the OH exposure can be calculated as follows:

$$[\text{OH}]\Delta t = \frac{1}{k_X - k_E} \left[ \ln\left(\frac{X}{E}\right)\Big|_{t=0} - \ln\left(\frac{X}{E}\right)\Big|_{t=t} \right] \quad (7)$$

in which  $k_X$  and  $k_E$  are the reaction rates of *m*, *p*-xylenes and ethylbenzene with OH radicals, respectively;  $\ln(X/E)|_{t=0}$  and  $\ln(X/E)|_{t=t}$  are the ratios of X/E for initial emission and observation, respectively.

As shown in Figure 2a, the concentrations of *m*, *p*-xylenes and ethylbenzene are highly correlated ( $r = 0.98$ ). The initial emission ratios of *m*, *p*-xylenes and ethylbenzene were estimated by different methods, such as the 95th or 90th percentile method [12,20], the nighttime mean method [44], and the nighttime highest concentration method [45]. In our study, we tried different methods to estimate the initial emission ratio. As depicted in Figure 2b, the ratio estimated by the regression of nighttime concentrations is 3.3, while the ratio estimated by the 90th percentile method is 3.7; the latter seems to be more reasonable. Finally, the determined initial emission ratio of *m*, *p*-xylenes to ethylbenzene was 3.7 ppbv/ppbv.

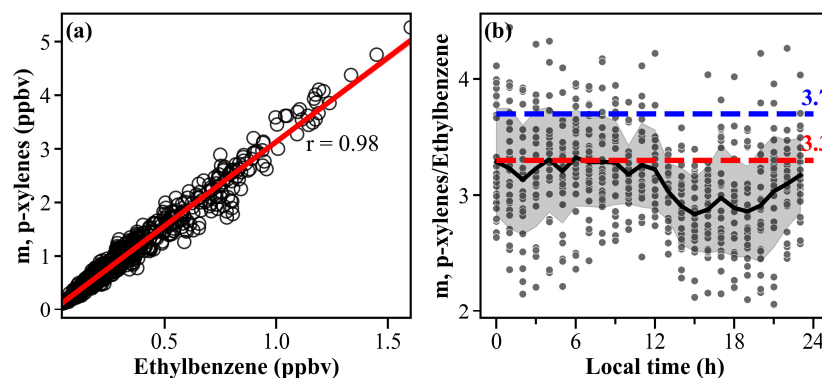


**Figure 2.** Scatterplot of measured *m*, *p*-xylene with ethylbenzene (a) and diurnal variation of the *m*, *p*-xylene/ethylbenzene ratios (b). The red dashed line represents the *m*, *p*-xylene/ethylbenzene initial emission ratio estimated by the regression of nighttime concentrations; the blue dashed line represents the initial ratio estimated by the 90th percentile method. The black line and grey areas are the mean and standard deviation, respectively.

### 3. Results and Discussion

#### 3.1. General Characteristics of Air Pollutants

Figure 3 shows the time series of  $\text{PM}_{2.5}$  and its carbonaceous components,  $\text{O}_3$ , and VOCs from 1–30 April 2019. During the observation period, the highest hourly concen-

tration of  $\text{PM}_{2.5}$  was  $114.1 \mu\text{g}/\text{m}^3$  (at 7:00 on 24 April), while the hourly  $\text{O}_3$  reached its maximum ( $245.3 \mu\text{g}/\text{m}^3$ ) at 16:00 on 24 April (Figure 3a). According to China's National Ambient Air Quality Standard (GB3095-2012), a haze pollution day was defined as a day with a daily average  $\text{PM}_{2.5}$  concentration exceeding  $75 \mu\text{g}/\text{m}^3$  (the secondary standard threshold for daily average  $\text{PM}_{2.5}$  concentration), and an  $\text{O}_3$  pollution day was defined as a condition with a daily maximum 8 h average (MDA8)  $\text{O}_3$  concentration greater than  $160 \mu\text{g}/\text{m}^3$  (the secondary standard threshold for MDA8  $\text{O}_3$ ). A CoP day was defined as a day when  $\text{PM}_{2.5}$  pollution and  $\text{O}_3$  pollution were present at the same time. In order to cover the entire pollution process, days with  $\text{PM}_{2.5}$  greater than  $35 \mu\text{g}/\text{m}^3$  during the development and dissipation phases of pollution were also considered. Based on the above definitions, there were two typical pollution episodes during our observation period: an SPP episode from 16–20 April 2019 and a CoP episode from 22–27 April 2019. As shown in Figure 3f, the end of these two pollution processes was significantly associated with the precipitation at noon on 20 April and at midnight on 28 April, respectively, indicating the beneficial effects of wet scavenging on spring air pollution.

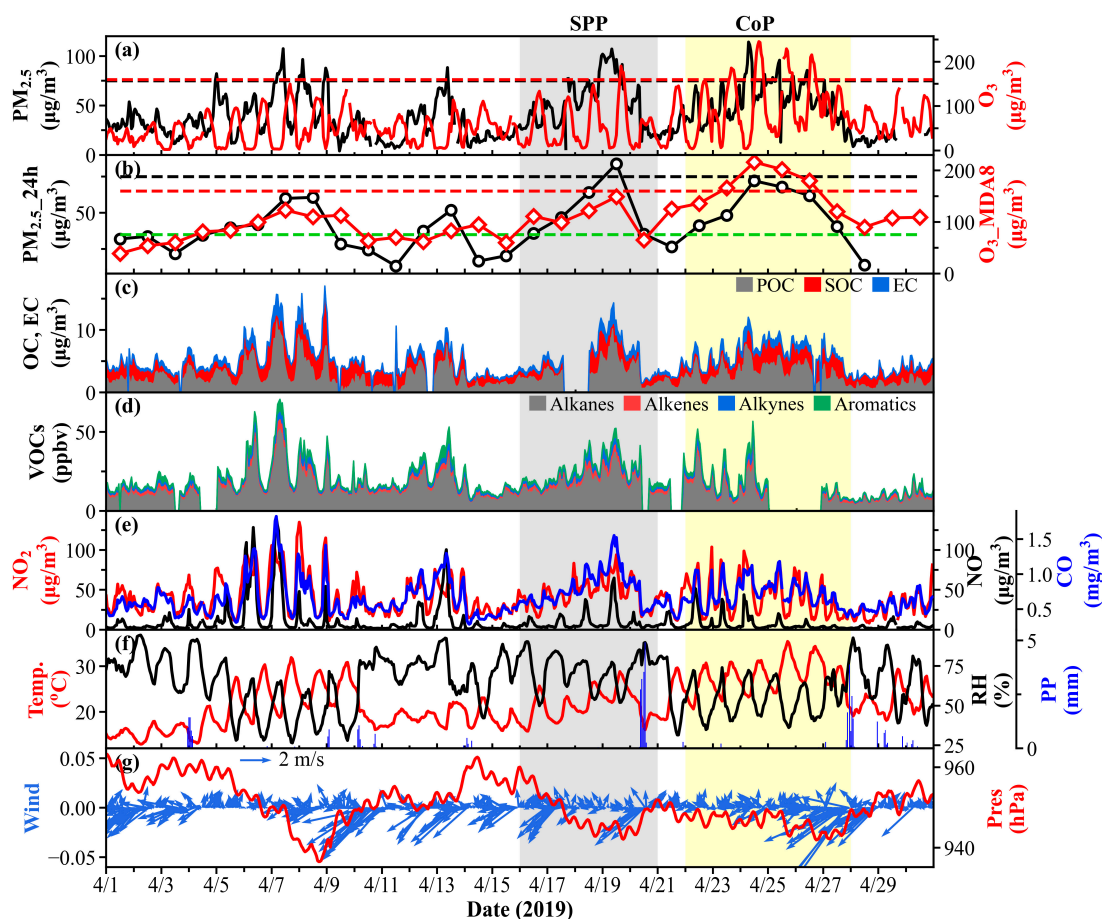


**Figure 3.** Time series of  $\text{PM}_{2.5}$  (a,b) and its carbonaceous components (c),  $\text{O}_3$  (a,b), VOCs (d), other gaseous pollutants (e), and meteorological parameters (f,g). The grey and yellow areas represent the SPP and CoP episodes, respectively.

Table 1 lists the mean values of each measured parameter for different pollution episodes. In general,  $\text{PM}_{2.5}$  concentrations were comparable during the two pollution episodes, with average concentrations of  $53.2 \pm 24.7 \mu\text{g}/\text{m}^3$  (SPP) and  $55.3 \pm 19.6 \mu\text{g}/\text{m}^3$  (CoP), respectively; however,  $\text{O}_3$  concentration in CoP ( $97.7 \pm 63.9 \mu\text{g}/\text{m}^3$ ) was approximately twice as high as in SPP ( $54.3 \pm 46.7 \mu\text{g}/\text{m}^3$ ), indicating that the atmospheric environment of the CoP was more oxidative. Meanwhile, the SOA concentration in CoP ( $6.5 \pm 2.6 \mu\text{g}/\text{m}^3$ ) was also much higher than that in SPP ( $4.3 \pm 3.2 \mu\text{g}/\text{m}^3$ ). More precisely,

SOA generation in CoP increased by 51.2% as compared to SPP, highlighting the intense SOA generation in CoP. In addition, VOCs, an important precursor of SOA and O<sub>3</sub>, were at lower levels in CoP ( $34.4 \pm 20.0$  ppbv) than in SPP ( $44.8 \pm 16.1$  ppbv), which may be related to the stronger photochemical consumption during the CoP period. However, as for EC and CO, which are mainly derived from primary combustion processes [46], their concentrations during the two pollution episodes were very close, showing that emissions from combustion sources did not change much.

**Table 1.** Statistical summary (mean  $\pm$  std) of measured air pollutants, carbonaceous components in PM<sub>2.5</sub>, VOC, and meteorological parameters in this study.

	Whole Period (1–30 April 2019) <sup>1</sup>	SPP (16–20 April 2019) <sup>1</sup>	CoP (22–27 April 2019) <sup>1</sup>
Air pollutants			
PM <sub>2.5</sub> (µg/m <sup>3</sup> )	40.6 $\pm$ 22.9	53.2 $\pm$ 24.7	55.3 $\pm$ 19.6
O <sub>3</sub> (µg/m <sup>3</sup> )	59.9 $\pm$ 47.8	54.3 $\pm$ 46.7	97.7 $\pm$ 63.9
MDA8 O <sub>3</sub> (µg/m <sup>3</sup> )	106.5 $\pm$ 42.6	109.2 $\pm$ 27.6	170.0 $\pm$ 33.9
NO <sub>2</sub> (µg/m <sup>3</sup> )	41.2 $\pm$ 22.3	46.1 $\pm$ 17.1	43.0 $\pm$ 23.6
NO (µg/m <sup>3</sup> )	10.0 $\pm$ 18.1	9.4 $\pm$ 11.0	7.5 $\pm$ 9.9
CO (mg/m <sup>3</sup> )	0.7 $\pm$ 0.2	0.8 $\pm$ 0.2	0.7 $\pm$ 0.2
Carbonaceous components in PM <sub>2.5</sub>			
POA (µg/m <sup>3</sup> )	5.3 $\pm$ 3.7	6.8 $\pm$ 4.1	6.6 $\pm$ 3.1
SOA (µg/m <sup>3</sup> )	5.6 $\pm$ 3.2	4.3 $\pm$ 3.2	6.5 $\pm$ 2.6
EC (µg/m <sup>3</sup> )	1.1 $\pm$ 0.8	1.5 $\pm$ 0.9	1.4 $\pm$ 0.7
Measured VOCs			
TVOCs (ppbv) <sup>2</sup>	36.2 $\pm$ 19.8	44.8 $\pm$ 16.1	34.4 $\pm$ 20.0
Alkanes (ppbv)	24.5 $\pm$ 14.1	31.1 $\pm$ 11.4	21.8 $\pm$ 14.2
Alkenes (ppbv)	4.1 $\pm$ 1.7	4.4 $\pm$ 1.3	4.3 $\pm$ 1.7
Alkynes (ppbv)	3.1 $\pm$ 2.2	4.5 $\pm$ 2.9	3.2 $\pm$ 1.9
Aromatics (ppbv)	4.4 $\pm$ 3.1	4.8 $\pm$ 2.1	5.0 $\pm$ 3.4
Meteorological parameters			
T (°C)	22.1 $\pm$ 4.9	21.5 $\pm$ 3.2	27.7 $\pm$ 3.4
T <sub>max</sub> (°C) <sup>3</sup>	26.3 $\pm$ 5.0	25.7 $\pm$ 1.9	32.2 $\pm$ 1.9
RH (%)	63.9 $\pm$ 16.1	72.4 $\pm$ 10.7	54.6 $\pm$ 10.8
WS (m/s)	1.1 $\pm$ 0.9	1.0 $\pm$ 0.7	1.2 $\pm$ 1.2

<sup>1</sup> The corresponding dates for the whole period, SPP, and CoP. <sup>2</sup> The mixing ratios of total VOCs. <sup>3</sup> The daily maximum temperature.

Pollutant concentrations are highly correlated with meteorological conditions. As listed in Table 1, the average wind speed during both pollutant episodes was low ( $\sim 1$  m/s), but the relative humidity and temperature varied considerably. During the CoP, higher temperature ( $27.7 \pm 3.4$  °C) and moderate relative humidity ( $54.6 \pm 10.8\%$ ) were observed, which were favorable for the co-occurrence of O<sub>3</sub> and PM<sub>2.5</sub> pollution [8].

### 3.2. Characteristics of SOA in PM<sub>2.5</sub>

Figure 4 presents the scatter plots of SOA versus PM<sub>2.5</sub> for different pollution episodes. It can be clearly seen that SOA concentration increased with PM<sub>2.5</sub> (Figure 4a), suggesting that the generation of SOA promoted the increase of PM<sub>2.5</sub>; that is, the generation of SOA can promote the development of the spring haze pollution processes to some extent. Further analyses of the different episodes (Figure 4b,c) showed that the correlation between SOA and PM<sub>2.5</sub> was stronger during SPP ( $r = 0.59$ ) than CoP ( $r = 0.27$ ). In addition, high SOA concentrations during SPP were concentrated at high PM<sub>2.5</sub> levels ( $>50$  µg/m<sup>3</sup>), and some high values of SOA were also observed at very low O<sub>3</sub> concentrations, which may be attributed to the heterogeneous generation of SOA. However, during CoP, a high SOA

concentration often occurred with high  $O_3$  concentration, highlighting the homogeneous generation of SOA.

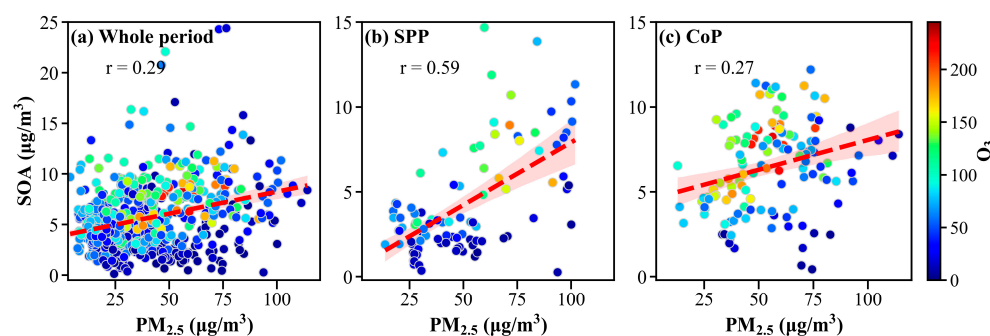


**Figure 4.** Scatter plots of the SOA and  $PM_{2.5}$  concentrations during different pollution episodes. (a) for the whole period, (b) for the SPP episode, and (c) for the CoP episode. The red dashed line in each subplot is the linear regression line of the scatter plot.

To further understand the generation of SOA in different types of pollution episodes, the diurnal patterns of different carbonaceous components during the two pollution episodes were also investigated (Figure 5). During the different pollution episodes, the diurnal trend of POA was relatively consistent, peaking in the morning rush hours (6:00–9:00) and rising again in the evening rush hours (Figure 5a). However, the diurnal trend of SOA varied greatly among the different pollution processes. As shown in Figure 5b, the SOA in the SPP exhibited a clear daytime bimodal feature, where the first peak may have been influenced by the strong photochemical oxidation in the afternoon, while the second peak may be due to the evening peak commute, during which large amounts of precursors are emitted into the atmosphere and can be oxidized by residual oxidants. The diurnal trend of SOA was not significant during the CoP, with high SOA concentrations throughout the day. Meanwhile, the nocturnal SOA concentrations were higher in CoP than in SPP, which may have been affected by the high level of  $O_3$  and high temperatures at night (Figure 5c,d). In addition, SOA in CoP also exhibited a bimodal peak during the day, with the peak shifting forward at noon as compared to SPP, which may be related to the rapid increase in daytime temperature and light intensity during the CoP episode. Once the light intensity is sufficient, a strong atmospheric photochemistry occurs, which then promotes the photooxidative production of SOA [47].

### 3.3. Characteristics of Measured VOCs in Different Pollution Episodes

As listed in Table 1, the average mixing ratio of total VOCs (TVOCs) during the whole observation period was  $36.2 \pm 19.8$  ppbv, which was higher than that in a previous study on Chengdu during the summer period ( $26.8 \pm 14.9$  ppbv) [32]. The levels of VOCs varied greatly among the different pollution episodes, with the mean mixing ratio of TVOCs in CoP ( $34.4 \pm 20.0$  ppbv) being only 76.8% of that in SPP ( $44.8 \pm 16.1$  ppbv). To further understand the characteristics of VOCs in different types of pollution episodes, this section will focus on comparing the composition, dominant species, and diurnal variation patterns as well as sources of VOCs during the two pollution episodes.

#### 3.3.1. Measured VOCs Composition and Dominant Species

As shown in Figure 6a,c, the concentrations of different VOC groups in SPP and CoP varied considerably. Overall, the concentrations of TVOCs in CoP decreased as compared to those in SPP, with significant decreases in alkanes (−29.8%, from 31.1 ppbv to 21.8 ppbv) and alkynes (−27.5%, from 4.6 ppbv to 3.2 ppbv), while alkenes (from 4.4 ppbv to 4.3 ppbv) and aromatics (from 4.8 ppbv to 5.0 ppbv) remained almost unchanged. Although the proportion of different VOC groups varied slightly from episode to episode, the ranking was always alkanes  $\gg$  aromatics > alkenes > alkynes. Figure 6b,d also displayed the top ten VOC species for both episodes. Ethane, n-decane, propane, 2-methylpentane, acetylene,

ethylene, iso-pentane, and iso-butane were always detected in the top ten VOC species during SPP and CoP. Almost all VOC species in CoP were at lower levels than in SPP, which may be related to the stronger atmospheric oxidation in CoP.

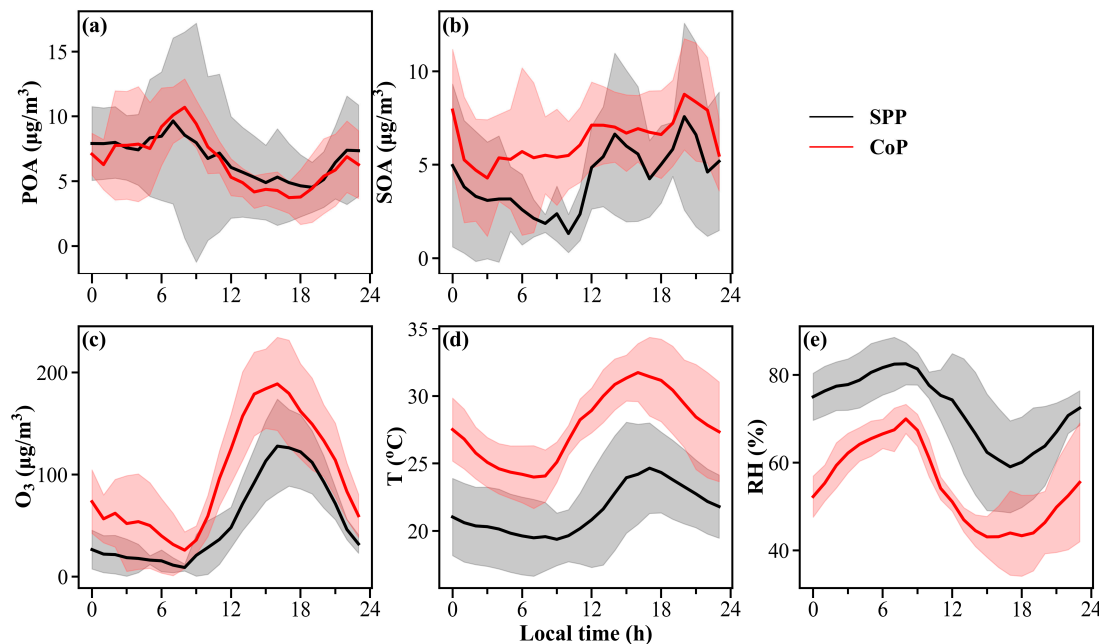


**Figure 5.** Diurnal patterns of different carbonaceous aerosols (a,b), O<sub>3</sub> (c), T (d) and RH (e) in different pollution episodes. The solid line and shaded areas are the mean and standard deviation, respectively.

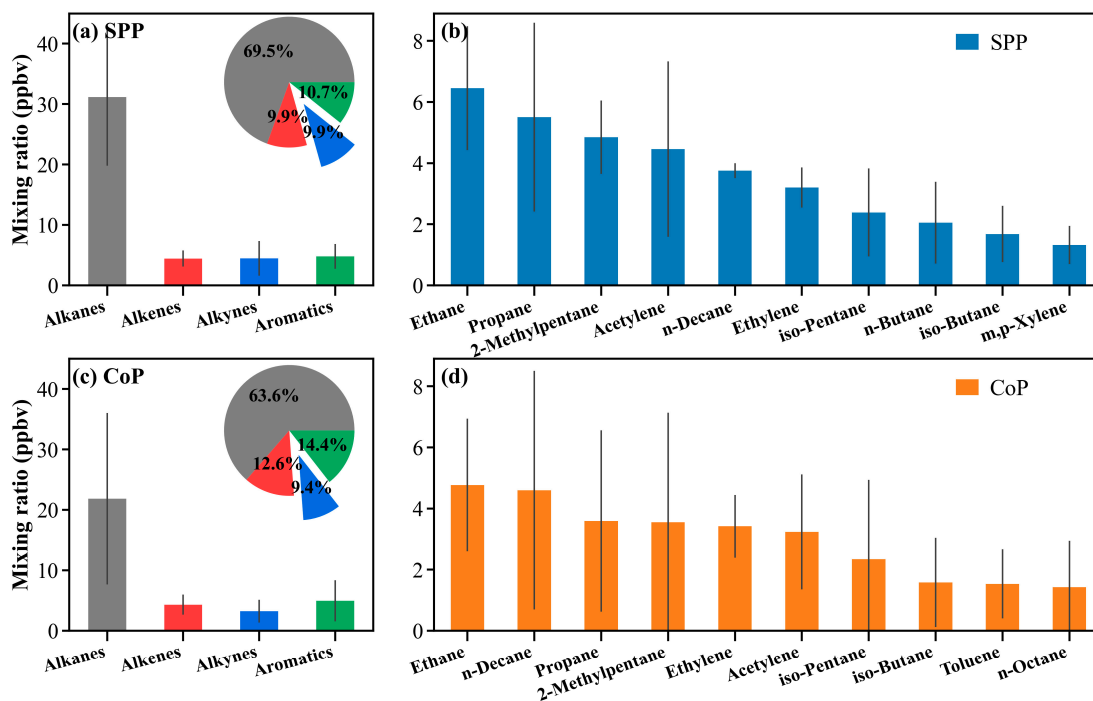


**Figure 6.** The VOC composition (a,c) and top 10 abundant species (b,d) in different pollution episodes. The error line on each bar corresponds to the standard deviation.

### 3.3.2. Diurnal Variations of VOC Groups

Figure 7 shows the diurnal variation of different VOCs groups, NO<sub>x</sub> (the sum of NO and NO<sub>2</sub>), O<sub>3</sub>, and O<sub>x</sub> (the sum of O<sub>3</sub> and NO<sub>2</sub>) for different pollution episodes. Overall,

the diurnal variation of VOCs was consistent with that of NO<sub>x</sub>, but the opposite of O<sub>3</sub>. As shown in Figure 7a,c, both NO<sub>x</sub> and VOCs exhibited a peak at around 9:00 in the morning in these two episodes, which may have been influenced by strong emissions and weak atmospheric oxidation during the morning peak commute (Figure 7h). After the morning peak hour, VOCs in CoP continued to decrease until 18:00 and then increased again. Additionally, we observed that the peak of VOCs in SPP lasted for several hours (9:00–12:00), while the VOCs in CoP peaked only at around 9:00 and then decreased rapidly. This phenomenon may be influenced by the different diurnal patterns of light intensity in the different episodes. Furthermore, the levels of VOCs in CoP were lower than those in SPP at most moments, which may be due to the high levels of Ox in CoP. We also found that the peaks of O<sub>3</sub> and Ox appeared earlier in CoP than in SPP, which were probably affected by the difference in diurnal temperature and the light variations in these two episodes (Figure 5e).

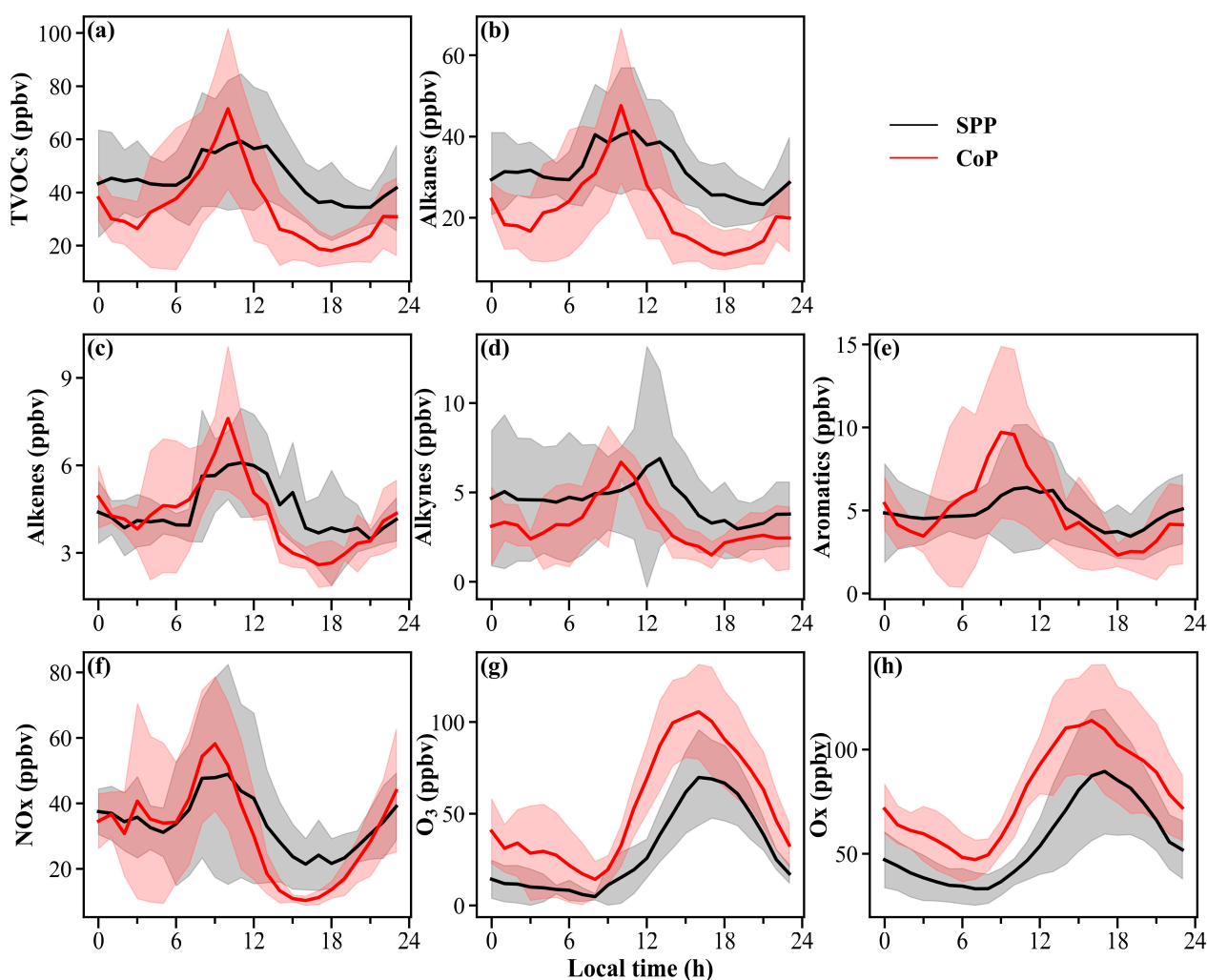


**Figure 7.** Diurnal patterns of VOCs (a–e), NO<sub>x</sub> (f), O<sub>3</sub> (g), and Ox (h) in different pollution episodes. The solid line and shaded areas are the mean and standard deviation, respectively.

### 3.3.3. Source Analysis of VOCs Based on Species-Specific Ratios

The ratios of some specific species pairs can be applied to preliminarily determine the VOC emission sources [48–50]. For example, the toluene/benzene ratio is commonly used to identify the sources of traffic emissions, fuel combustion, and industrial and solvent usage [51,52]; the isopentane/n-pentane ratio can also be used to indicate different sources, including traffic emissions, coal combustion, liquid gasoline, and fuel volatilization [53].

The ratios of different species pairs from different sources have been summarized by Shi and co-authors [49].

The ratios of different species pairs in this study for different pollution episodes and other research works are listed in Table 2. The benzene/toluene ratios for SPP and CoP were  $0.86 \pm 1.57$  and  $0.75 \pm 0.60$ , respectively, which were slightly higher than those for vehicle exhaust emissions (0.56–0.60), indicating the contribution of other high-rate sources (e.g., coal combustion emissions and biomass burning), especially for the SPP episode. The isopentane/n-pentane ratios varied significantly in SPP and CoP, with mean values of  $2.65 \pm 0.70$  and  $3.42 \pm 1.12$ , respectively. The high isopentane/n-pentane ratios suggest that VOCs in urban Chengdu are mainly influenced by vehicle emission and fuel volatilization, with the isopentane/n-pentane ratios from these sources being 2.93 and 1.84–4.46, respectively. The extremely high isopentane/n-pentane ratio in CoP emphasizes the high contribution of volatile sources, including gasoline and fuel volatilization, which may be related to the high temperature that promotes oil and gas evaporation during this period.

**Table 2.** Ratios of different VOC species pairs in this study for different pollution episodes and other research works.

	Benzene/Toluene	Isopentane/n-Pentane
	This study	
SPP (2019.4.16–4.20)	$0.86 \pm 1.57$ <sup>1</sup>	$2.65 \pm 0.70$ <sup>2</sup>
CoP (2019.4.22–4.27)	$0.75 \pm 0.60$ <sup>1</sup>	$3.42 \pm 1.12$ <sup>2</sup>
	Previous studies	
Solvent usage	0.00–0.20 <sup>3</sup>	
Biomass burning	2.50 <sup>3</sup>	
Vehicle emission	0.56–0.60 <sup>3</sup>	2.93 <sup>4</sup>
Coal combustion	1.05–2.20 <sup>3</sup>	0.56–0.80 <sup>4</sup>
Natural gas		0.82–0.89 <sup>5</sup>
Liquid gasoline		1.50–3.00 <sup>5</sup>
Fuel volatilization		1.84–4.46 <sup>5</sup>

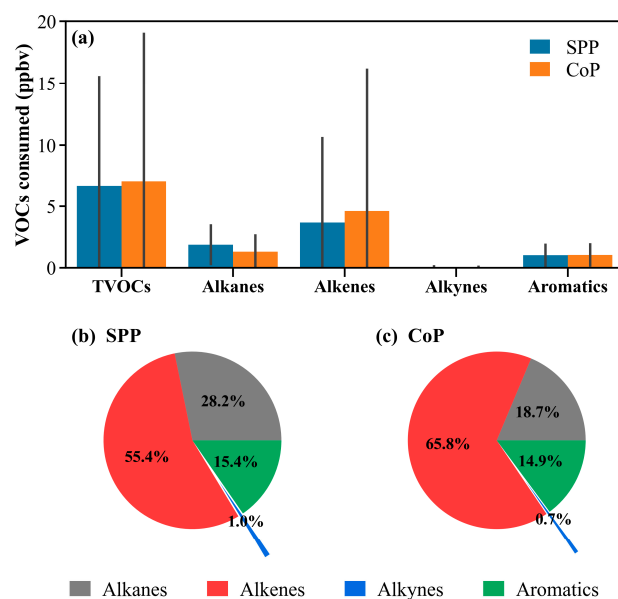
<sup>1</sup> Ratios of benzene to toluene in this study. <sup>2</sup> Ratios of isopentane to n-pentane in this study. <sup>3</sup> Ratios of benzene to toluene in different emission sources, with reference to Zhang and co-authors [53]. <sup>4</sup> and <sup>5</sup> Ratios of isopentane to n-pentane in different emission sources, with reference to Yan and co-authors [54], and Zheng and co-authors [55], respectively.

### 3.4. Characteristics of Consumed VOCs in Different Pollution Episodes

It is well-known that VOCs are one of the important precursors of tropospheric O<sub>3</sub> [38]. Once VOCs are emitted by emission sources, they undergo photochemical consumption during their subsequent transport. Zhan et al. [56] reported that the photochemical consumption of VOCs is strongly associated with the formation of O<sub>3</sub> and SOA. Thus, to further investigate the VOCs consumed and their contribution to SOA in different pollution episodes, VOC consumption was estimated based on the assumption that the oxidation of OH radicals dominate the loss of VOCs in the ambient atmosphere. A detailed description of the estimation steps can be found in Section 2.3.2.

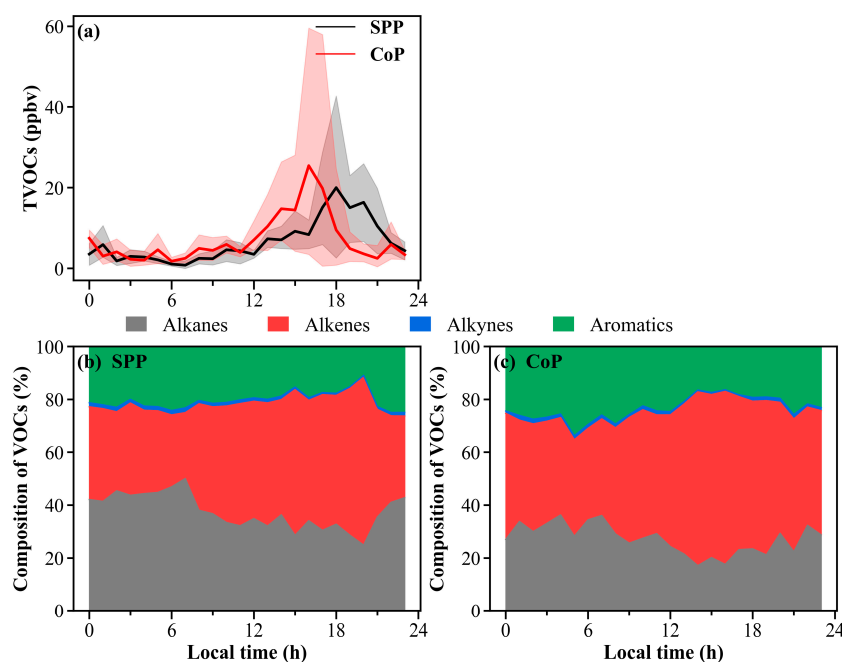
#### 3.4.1. Composition and Diurnal Patterns of Consumed VOCs

Figure 8 shows the average concentration and composition of the VOCs consumed during the SPP and CoP. As can be seen in Figure 8a, the total VOCs consumed during CoP ( $7.0 \pm 12.1$  ppbv) were slightly higher than those during SPP ( $6.6 \pm 8.9$  ppbv), mainly due to the high consumption of alkenes in CoP. In addition, the composition of consumed VOCs differed from the composition of measured VOCs (ranked as alkanes >> aromatics > alkenes > alkynes), and the largest proportion of the consumed VOCs consisted of alkenes (55.4–65.8%), followed by alkanes (18.7% to 28.2%), and aromatics (14.9% to 15.4%).



**Figure 8.** Concentration (a) and composition (b,c) of consumed VOCs in different pollution episodes. The error line on each bar corresponds to the standard deviation.

Figure 9 also presents the diurnal patterns of the total concentration and composition of the consumed VOCs. The consumption of VOCs exhibited different diurnal patterns in different pollution episodes. Overall, the total VOCs consumed in the two episodes showed a clear unimodal trend, with the peak occurring after the O<sub>3</sub> peak and relatively close to the Ox peak. Meanwhile, the peak in CoP was obviously earlier than that in SPP. As for the diurnal variation in the composition of consumed VOCs (Figure 9b,c), a high percentage of alkenes appeared during the daytime, while high percentages of alkanes and aromatics occurred at night.



**Figure 9.** Diurnal pattern of TVOCs (a) and chemical composition (b,c) of consumed VOCs in different pollution episodes. The solid line and shaded areas in figure (a) are the mean and standard deviation, respectively.

### 3.4.2. Estimation of SOA Based on VOC Consumption

SOA estimation based on VOC consumption can reflect the potential of VOCs to form SOA through the photochemical oxidation pathway [12]. As shown in Figure 10a, SOA that can be produced through VOC consumption in SPP and CoP were  $1.1 \pm 0.9 \mu\text{g}/\text{m}^3$  and  $0.9 \pm 0.9 \mu\text{g}/\text{m}^3$ , respectively. Combined with Figure 8a, it can be seen that although the VOC consumption of CoP was higher than that of SPP, its SOA generation through VOC consumption was lower than that of SPP. This finding could be explained by the competing effects of other oxidants (e.g.,  $\text{NO}_3$  radical and  $\text{O}_3$ ) in CoP. On the one hand, the  $\text{O}_3$  concentration of CoP was about twice that of SPP, which may enhance the formation of  $\text{NO}_3$  radicals and thus promote the  $\text{NO}_3$  oxidation of VOCs; on the other hand, the high concentration of  $\text{O}_3$  may directly lead to the  $\text{O}_3$  oxidation of VOCs. To address this issue, the formation of SOA through the different oxidation pathways of VOCs can be systematically investigated in future studies.

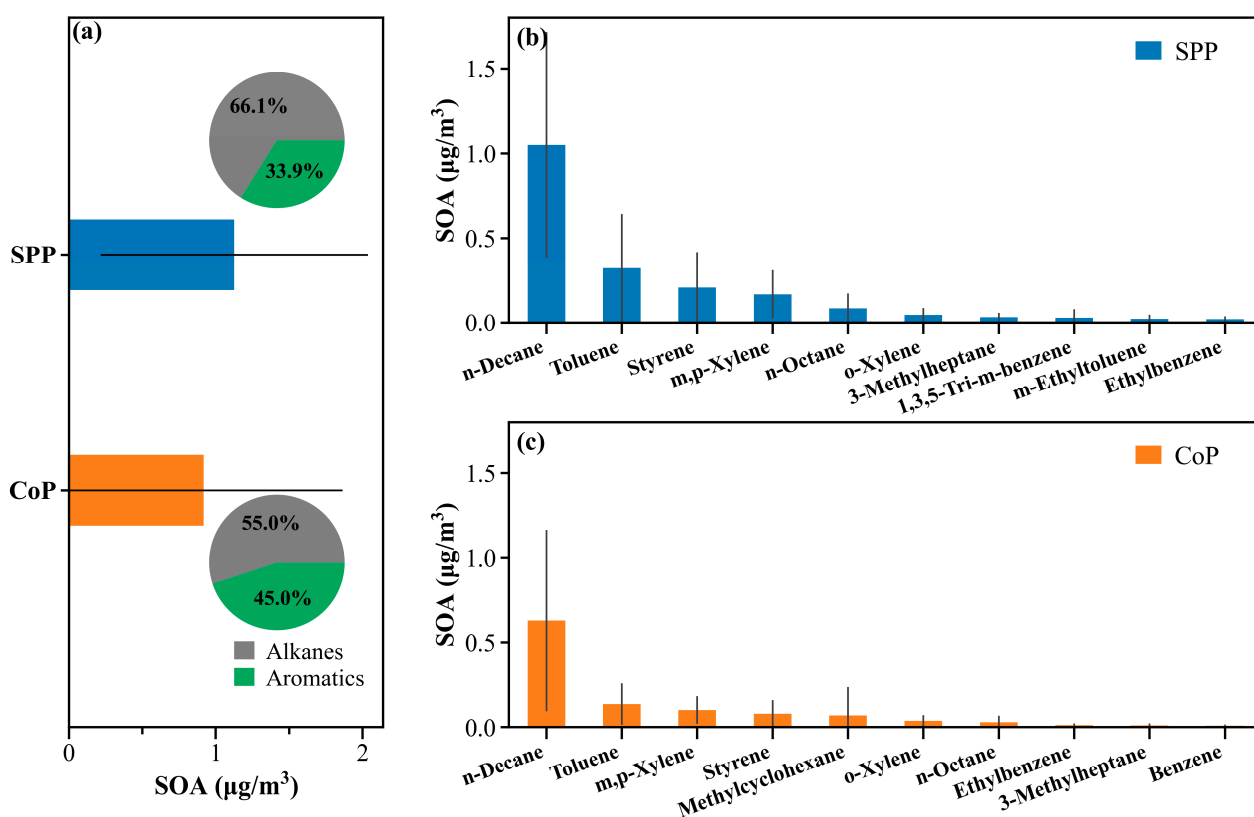


**Figure 10.** Comparison of SOA generation estimated from consumed VOCs in different pollution episodes (a) and the top ten 10 VOCs species forming SOA by photochemical oxidation (b,c). The error line on each bar corresponds to the standard deviation.

As shown in Figure 10b,c, the VOC species that contributed the most to SOA production according to the VOC consumption-based SOA yield method were n-decane, toluene, m,p-xylene, styrene, n-octane, o-xylene, and methylcyclohexane. A previous study conducted in Chengdu during the summer period reported that aromatic hydrocarbons, such as toluene, m,p-xylene, o-xylene, and ethylbenzene, contributed significantly to the estimated SOA potential based on the measured VOC concentrations [32]. However, our estimate of SOA based on VOC concentrations consumed by OH radicals also highlight the high contribution of high-carbon alkanes, such as n-decane and n-octane, to SOA formation. Therefore, in addition to reducing the emissions from aromatic hydrocarbons, mitigating the emissions of these high-carbon alkanes would also have a positive impact on the control of secondary organic pollution.

#### 4. Conclusions

In this study, the formation characteristics of SOA in different types of haze pollution in Chengdu were investigated. During the observation period, a CoP occurred immediately after an SPP, and the O<sub>3</sub> concentration in CoP was almost twice as high as that in SPP. The enhanced atmospheric oxidation during CoP resulted in a 51.2% increase in SOA concentrations as compared to the SPP. The lower measured VOC concentrations during the CoP also suggested that VOC consumption was greater in a highly oxidizing ambient atmosphere. Meanwhile, a slightly higher photochemical consumption of VOCs was derived during the CoP episode. However, the SOA produced through photochemical consumption showed a different profile as it was slightly lower in CoP. Furthermore, we found that some high-carbon alkanes (n-decane and n-octane) and aromatic hydrocarbons significantly contributed to SOA production in both pollution episodes. Thus, it is necessary to strengthen the control of these species in order to mitigate secondary organic pollution.

To some extent, our findings can help us to understand the formation of SOA in different types of pollution episodes. The biggest limitation of this study is that only one SPP episode and one CoP episode were included, which can provide a preliminary insight into SOA formation during different pollution episodes, but is not sufficient so as to provide an in-depth analysis of its causes. In the future, longer-term or multi-year measurements should be carried out to cover more pollution episodes and to further analyze the causes of high SOA concentrations in CoP episodes. Similar studies should also be conducted during the typical periods when only PM<sub>2.5</sub> pollution or only O<sub>3</sub> pollution is present, in order to explore the synergistic control of PM<sub>2.5</sub> and O<sub>3</sub> from multiple perspectives.

**Supplementary Materials:** The following supporting information can be downloaded at: <https://www.mdpi.com/article/10.3390/atmos13111834/s1>, Figure S1: Illustration of the use of the minimum R<sup>2</sup> method (MRS) to obtain (OC/EC)<sub>pri</sub>. Table S1: SOA yields of the VOC photochemical reaction in this study.

**Author Contributions:** Conceptualization, X.C.; methodology, T.S. and Y.L.; data curation, M.F. and D.S., writing—original draft preparation, T.S.; writing—review and editing, X.C. and Y.W.; visualization, T.S. and S.L.; supervision, Q.T. and F.Y. All authors have read and agreed to the published version of the manuscript.

**Funding:** This research was funded by the National Natural Science Foundation of China (Grant No. 42175124 and 41875162) and the Chengdu Science and Technology Bureau (Grant No. 2020-YF09-00051-SN).

**Institutional Review Board Statement:** Not applicable.

**Informed Consent Statement:** Not applicable.

**Data Availability Statement:** Not applicable.

**Acknowledgments:** We are grateful for the financial support from the National Natural Science Foundation of China (No. 42175124 and 41875162) and Chengdu Science and Technology Bureau (No. 2020-YF09-00051-SN). We would also like to extend our deep gratitude to the reviewers and editors who provided valuable comments to improve the quality of the paper.

**Conflicts of Interest:** The authors declare no conflict of interest.

#### References

1. Deng, C.; Tian, S.; Li, Z.W.; Li, K. Spatiotemporal characteristics of PM<sub>2.5</sub> and ozone concentrations in Chinese urban clusters. *Chemosphere* **2022**, *295*, 133813. [[CrossRef](#)]
2. Zhao, H.; Chen, K.; Liu, Z.; Zhang, Y.; Shao, T.; Zhang, H. Coordinated control of PM<sub>2.5</sub> and O<sub>3</sub> is urgently needed in China after implementation of the “Air pollution prevention and control action plan”. *Chemosphere* **2021**, *270*, 129441. [[CrossRef](#)]
3. State Council of the People’s Republic of China. *Air pollution Prevention and Control Action Plan 2013*; State Council of the People’s Republic of China: Beijing, China, 2013.
4. State Council of the People’s Republic of China. *Three-Year Action Plan of Win the Blue Sky Defence War 2018*; State Council of the People’s Republic of China: Beijing, China, 2018.

5. Zhai, S.; Jacob, D.J.; Wang, X.; Shen, L.; Li, K.; Zhang, Y.; Gui, K.; Zhao, T.; Liao, H. Fine particulate matter (PM<sub>2.5</sub>) trends in China, 2013–2018: Separating contributions from anthropogenic emissions and meteorology. *Atmos. Chem. Phys.* **2019**, *19*, 11031–11041. [[CrossRef](#)]
6. Li, K.; Jacob, D.J.; Liao, H.; Zhu, J.; Shah, V.; Shen, L.; Bates, K.H.; Zhang, Q.; Zhai, S. A two-pollutant strategy for improving ozone and particulate air quality in China. *Nat. Geosci.* **2019**, *12*, 906–910. [[CrossRef](#)]
7. Zhao, S.; Yu, Y.; Yin, D.; Qin, D.; He, J.; Dong, L. Spatial patterns and temporal variations of six criteria air pollutants during 2015 to 2017 in the city clusters of Sichuan Basin, China. *Sci. Total Environ.* **2018**, *624*, 540–557. [[CrossRef](#)]
8. Dai, H.; Zhu, J.; Liao, H.; Li, J.; Liang, M.; Yang, Y.; Yue, X. Co-occurrence of ozone and PM<sub>2.5</sub> pollution in the Yangtze River Delta over 2013–2019: Spatiotemporal distribution and meteorological conditions. *Atmos. Res.* **2021**, *249*, 105363. [[CrossRef](#)]
9. He, Y.; Li, L.; Wang, H.; Xu, X.; Li, Y.; Fan, S. A cold front induced co-occurrence of O<sub>3</sub> and PM<sub>2.5</sub> pollution in a Pearl River Delta city: Temporal variation, vertical structure, and mechanism. *Environ. Pollut.* **2022**, *306*, 119464. [[CrossRef](#)]
10. Luo, Y.; Zhao, T.; Yang, Y.; Zong, L.; Kumar, K.R.; Wang, H.; Meng, K.; Zhang, L.; Lu, S.; Xin, Y. Seasonal changes in the recent decline of combined high PM<sub>2.5</sub> and O<sub>3</sub> pollution and associated chemical and meteorological drivers in the Beijing–Tianjin–Hebei region, China. *Sci. Total Environ.* **2022**, *838*, 156312. [[CrossRef](#)]
11. Hallquist, M.; Wenger, J.C.; Baltensperger, U.; Rudich, Y.; Simpson, D.; Claeys, M.; Dommen, J.; Donahue, N.M.; George, C.; Goldstein, A.H.; et al. The formation, properties and impact of secondary organic aerosol: Current and emerging issues. *Atmos. Chem. Phys.* **2009**, *9*, 5155–5236. [[CrossRef](#)]
12. Wang, H.; Wang, Q.; Gao, Y.; Zhou, M.; Jing, S.; Qiao, L.; Yuan, B.; Huang, D.; Huang, C.; Lou, S.; et al. Estimation of Secondary Organic Aerosol Formation During a Photochemical Smog Episode in Shanghai, China. *J. Geophys. Res. Atmos.* **2020**, *125*, e2019JD032033. [[CrossRef](#)]
13. Li, Q.; Su, G.; Li, C.; Liu, P.; Zhao, X.; Zhang, C.; Sun, X.; Mu, Y.; Wu, M.; Wang, Q.; et al. An investigation into the role of VOCs in SOA and ozone production in Beijing, China. *Sci. Total Environ.* **2020**, *720*, 137536. [[CrossRef](#)]
14. Wang, T.; Xue, L.; Brimblecombe, P.; Lam, Y.F.; Li, L.; Zhang, L. Ozone pollution in China: A review of concentrations, meteorological influences, chemical precursors, and effects. *Sci. Total Environ.* **2017**, *575*, 1582–1596. [[CrossRef](#)]
15. Lu, K.; Guo, S.; Tan, Z.; Wang, H.; Shang, D.; Liu, Y.; Li, X.; Wu, Z.; Hu, M.; Zhang, Y. Exploring atmospheric free-radical chemistry in China: The self-cleansing capacity and the formation of secondary air pollution. *Natl. Sci. Rev.* **2019**, *6*, 579–594. [[CrossRef](#)]
16. Wu, C.; Yu, J.Z. Determination of primary combustion source organic carbon-to-elemental carbon (OC / EC) ratio using ambient OC and EC measurements: Secondary OC-EC correlation minimization method. *Atmos. Chem. Phys.* **2016**, *16*, 5453–5465. [[CrossRef](#)]
17. Guo, S.; Hu, M.; Guo, Q.; Shang, D. Comparison of Secondary Organic Aerosol Estimation Methods. *Acta Chim. Sinica* **2014**, *72*, 658–666. [[CrossRef](#)]
18. Ren, H.; Hu, W.; Wei, L.; Yue, S.; Zhao, J.; Li, L.; Wu, L.; Zhao, W.; Ren, L.; Kang, M.; et al. Measurement report: Vertical distribution of biogenic and anthropogenic secondary organic aerosols in the urban boundary layer over Beijing during late summer. *Atmos. Chem. Phys.* **2021**, *21*, 12949–12963. [[CrossRef](#)]
19. Yang, C.; Hong, Z.; Chen, J.; Xu, L.; Zhuang, M.; Huang, Z. Characteristics of secondary organic aerosols tracers in PM<sub>2.5</sub> in three central cities of the Yangtze river delta, China. *Chemosphere* **2022**, *293*, 133637. [[CrossRef](#)]
20. Zheng, H.; Kong, S.; Chen, N.; Niu, Z.; Zhang, Y.; Jiang, S.; Yan, Y.; Qi, S. Source apportionment of volatile organic compounds: Implications to reactivity, ozone formation, and secondary organic aerosol potential. *Atmos. Res.* **2021**, *249*, 105344. [[CrossRef](#)]
21. Zhao, S.; Yin, D.; Yu, Y.; Kang, S.; Qin, D.; Dong, L. PM<sub>2.5</sub> and O<sub>3</sub> pollution during 2015–2019 over 367 Chinese cities: Spatiotemporal variations, meteorological and topographical impacts. *Environ. Pollut.* **2020**, *264*, 114694. [[CrossRef](#)]
22. Huang, X.; Zhang, J.K.; Luo, B.; Wang, L.L.; Tang, G.Q.; Liu, Z.R.; Song, H.Y.; Zhang, W.; Yuan, L.; Wang, Y.S. Water-soluble ions in PM<sub>2.5</sub> during spring haze and dust periods in Chengdu, China: Variations, nitrate formation and potential source areas. *Environ. Pollut.* **2018**, *243*, 1740–1749. [[CrossRef](#)]
23. Li, L.; Tan, Q.W.; Zhang, Y.H.; Feng, M.; Qu, Y.; An, J.L.; Liu, X.G. Characteristics and source apportionment of PM<sub>2.5</sub> during persistent extreme haze events in Chengdu, southwest China. *Environ. Pollut.* **2017**, *230*, 718–729. [[CrossRef](#)]
24. Tian, M.; Liu, Y.; Yang, F.; Zhang, L.; Peng, C.; Chen, Y.; Shi, G.; Wang, H.; Luo, B.; Jiang, C.; et al. Increasing importance of nitrate formation for heavy aerosol pollution in two megacities in Sichuan Basin, southwest China. *Environ. Pollut.* **2019**, *250*, 898–905. [[CrossRef](#)]
25. Song, T.; Feng, M.; Song, D.; Zhou, L.; Qiu, Y.; Tan, Q.; Yang, F. Enhanced nitrate contribution during winter haze events in a megacity of Sichuan Basin, China: Formation mechanism and source apportionment. *J. Clean. Prod.* **2022**, *370*, 133272. [[CrossRef](#)]
26. Yang, X.; Wu, K.; Wang, H.; Liu, Y.; Gu, S.; Lu, Y.; Zhang, X.; Hu, Y.; Ou, Y.; Wang, S.; et al. Summertime ozone pollution in Sichuan Basin, China: Meteorological conditions, sources and process analysis. *Atmos. Environ.* **2020**, *226*, 117392. [[CrossRef](#)]
27. Yang, Y.; Li, X.; Zu, K.; Lian, C.; Chen, S.; Dong, H.; Feng, M.; Liu, H.; Liu, J.; Lu, K.; et al. Elucidating the effect of HONO on O<sub>3</sub> pollution by a case study in southwest China. *Sci. Total Environ.* **2021**, *756*, 144127. [[CrossRef](#)]
28. Tan, Z.; Lu, K.D.; Jiang, M.Q.; Su, R.; Dong, H.B.; Zeng, L.M.; Xie, S.D.; Tan, Q.W.; Zhang, Y.H. Exploring ozone pollution in Chengdu, southwestern China: A case study from radical chemistry to O<sub>3</sub>-VOC-NO<sub>x</sub> sensitivity. *Sci. Total Environ.* **2018**, *636*, 775–786. [[CrossRef](#)]
29. Deng, Y.; Li, J.; Li, Y.Q.; Wu, R.R.; Xie, S.D. Characteristics of volatile organic compounds, NO<sub>2</sub>, and effects on ozone formation at a site with high ozone level in Chengdu. *J. Environ. Sci.* **2019**, *75*, 334–345. [[CrossRef](#)]

30. Kong, L.; Feng, M.; Liu, Y.; Zhang, Y.; Zhang, C.; Li, C.; Qu, Y.; An, J.; Liu, X.; Tan, Q.; et al. Elucidating the pollution characteristics of nitrate, sulfate and ammonium in PM<sub>2.5</sub> in Chengdu, southwest China, based on 3-year measurements. *Atmos. Chem. Phys.* **2020**, *20*, 11181–11199. [[CrossRef](#)]
31. Kong, L.; Tan, Q.W.; Feng, M.; Qu, Y.; An, J.L.; Liu, X.G.; Cheng, N.L.; Deng, Y.J.; Zhai, R.X.; Wang, Z. Investigating the characteristics and source analyses of PM<sub>2.5</sub> seasonal variations in Chengdu, Southwest China. *Chemosphere* **2020**, *243*, 125267. [[CrossRef](#)]
32. Xiong, C.; Wang, N.; Zhou, L.; Yang, F.; Qiu, Y.; Chen, J.; Han, L.; Li, J. Component characteristics and source apportionment of volatile organic compounds during summer and winter in downtown Chengdu, southwest China. *Atmos. Environ.* **2021**, *258*, 118485. [[CrossRef](#)]
33. Zhao, S.; Yu, Y.; Qin, D.H.; Yin, D.Y.; Dong, L.X.; He, J.J. Analyses of regional pollution and transportation of PM<sub>2.5</sub> and ozone in the city clusters of Sichuan Basin, China. *Atmos. Pollut. Res.* **2019**, *10*, 374–385. [[CrossRef](#)]
34. Song, M.; Liu, X.G.; Tan, Q.W.; Feng, M.; Qu, Y.; An, J.L.; Zhang, Y.H. Characteristics and formation mechanism of persistent extreme haze pollution events in Chengdu, southwestern China. *Environ. Pollut.* **2019**, *251*, 1–12. [[CrossRef](#)]
35. Song, M.; Tan, Q.; Feng, M.; Qu, Y.; Liu, X.; An, J.; Zhang, Y. Source Apportionment and Secondary Transformation of Atmospheric Nonmethane Hydrocarbons in Chengdu, Southwest China. *J. Geophys. Res. Atmos.* **2018**, *123*, 9741–9763. [[CrossRef](#)]
36. Turpin, B.J.; Huntzicker, J.J. Identification of secondary organic aerosol episodes and quantitation of primary and secondary organic aerosol concentrations during SCAQS. *Atmos. Environ.* **1995**, *29*, 3527–3544. [[CrossRef](#)]
37. Hu, W.; Hu, M.; Hu, W.-W.; Niu, H.; Zheng, J.; Wu, Y.; Chen, W.; Chen, C.; Li, L.; Shao, M.; et al. Characterization of submicron aerosols influenced by biomass burning at a site in the Sichuan Basin, southwestern China. *Atmos. Chem. Phys.* **2016**, *16*, 13213–13230. [[CrossRef](#)]
38. Seinfeld, J.H.; Pandis, S.N. *Atmospheric Chemistry and Physics: From Air Pollution to Climate Change*; John Wiley & Sons: Hoboken, NJ, USA, 2006.
39. Ng, N.L.; Kroll, J.H.; Chan, A.W.H.; Chhabra, P.S.; Flagan, R.C.; Seinfeld, J.H. Secondary organic aerosol formation from m-xylene, toluene, and benzene. *Atmos. Chem. Phys.* **2007**, *7*, 3909–3922. [[CrossRef](#)]
40. Lim, Y.B.; Ziemann, P.J. Effects of Molecular Structure on Aerosol Yields from OH Radical-Initiated Reactions of Linear, Branched, and Cyclic Alkanes in the Presence of NO<sub>x</sub>. *Environ. Sci. Technol.* **2009**, *43*, 2328–2334. [[CrossRef](#)]
41. Zhang, X.; Cappa, C.D.; Jathar, S.H.; McVay, R.C.; Ensberg, J.J.; Kleeman, M.J.; Seinfeld, J.H. Influence of vapor wall loss in laboratory chambers on yields of secondary organic aerosol. *Proc. Natl. Acad. Sci. USA* **2014**, *111*, 5802–5807. [[CrossRef](#)]
42. Shao, M.; Wang, B.; Lu, S.; Yuan, B.; Wang, M. Effects of Beijing Olympics Control Measures on Reducing Reactive Hydrocarbon Species. *Environ. Sci. Technol.* **2011**, *45*, 514–519. [[CrossRef](#)]
43. Wu, C.; Wang, C.; Wang, S.; Wang, W.; Yuan, B.; Qi, J.; Wang, B.; Wang, H.; Wang, C.; Song, W.; et al. Measurement report: Important contributions of oxygenated compounds to emissions and chemistry of volatile organic compounds in urban air. *Atmos. Chem. Phys.* **2020**, *20*, 14769–14785. [[CrossRef](#)]
44. Zou, Y.; Charlesworth, E.; Wang, N.; Flores, R.M.; Liu, Q.Q.; Li, F.; Deng, T.; Deng, X.J. Characterization and ozone formation potential (OFP) of non-methane hydrocarbons under the condition of chemical loss in Guangzhou, China. *Atmos. Environ.* **2021**, *262*, 118630. [[CrossRef](#)]
45. Yuan, B.; Hu, W.W.; Shao, M.; Wang, M.; Chen, W.T.; Lu, S.H.; Zeng, L.M.; Hu, M. VOC emissions, evolutions and contributions to SOA formation at a receptor site in eastern China. *Atmos. Chem. Phys.* **2013**, *13*, 8815–8832. [[CrossRef](#)]
46. Wang, H.; Tian, M.; Chen, Y.; Shi, G.; Liu, Y.; Yang, F.; Zhang, L.; Deng, L.; Yu, J.; Peng, C.; et al. Seasonal characteristics, formation mechanisms and source origins of PM<sub>2.5</sub> in two megacities in Sichuan Basin, China. *Atmos. Chem. Phys.* **2018**, *18*, 865–881. [[CrossRef](#)]
47. Sbai, S.E.; Li, C.; Boreave, A.; Charbonnel, N.; Perrier, S.; Vernoux, P.; Bentayeb, F.; George, C.; Gil, S. Atmospheric photochemistry and secondary aerosol formation of urban air in Lyon, France. *J. Environ. Sci.* **2021**, *99*, 311–323. [[CrossRef](#)] [[PubMed](#)]
48. Li, J.; Deng, S.; Li, G.; Lu, Z.; Song, H.; Gao, J.; Sun, Z.; Xu, K. VOCs characteristics and their ozone and SOA formation potentials in autumn and winter at Weinan, China. *Environ. Res.* **2022**, *203*, 111821. [[CrossRef](#)] [[PubMed](#)]
49. Shi, J.; Bao, Y.; Xiang, F.; Wang, Z.; Ren, L.; Pang, X.; Wang, J.; Han, X.; Ning, P. Pollution Characteristics and Health Risk Assessment of VOCs in Jinghong. *Atmosphere* **2022**, *13*, 613. [[CrossRef](#)]
50. Niu, Y.; Yan, Y.; Chai, J.; Zhang, X.; Xu, Y.; Duan, X.; Wu, J.; Peng, L. Effects of regional transport from different potential pollution areas on volatile organic compounds (VOCs) in Northern Beijing during non-heating and heating periods. *Sci. Total Environ.* **2022**, *836*, 155465. [[CrossRef](#)]
51. Zhang, L.; Li, H.; Wu, Z.; Zhang, W.; Liu, K.; Cheng, X.; Zhang, Y.; Li, B.; Chen, Y. Characteristics of atmospheric volatile organic compounds in urban area of Beijing: Variations, photochemical reactivity and source apportionment. *J. Environ. Sci.* **2020**, *95*, 190–200. [[CrossRef](#)]
52. Kumar, A.; Singh, D.; Kumar, K.; Singh, B.B.; Jain, V.K. Distribution of VOCs in urban and rural atmospheres of subtropical India: Temporal variation, source attribution, ratios, OFP and risk assessment. *Sci. Total Environ.* **2018**, *613–614*, 492–501. [[CrossRef](#)]
53. Zhang, Y.; Yin, S.; Yuan, M.; Zhang, R.; Zhang, M.; Yu, S.; Li, Y. Characteristics and source apportionment of ambient VOC in spring in Zhengzhou. *Environ. Sci.* **2019**, *40*, 4372–4381. [[CrossRef](#)]

54. Yan, Y.; Peng, L.; Li, R.; Li, Y.; Li, L.; Bai, H. Concentration, ozone formation potential and source analysis of volatile organic compounds (VOCs) in a thermal power station centralized area: A study in Shuozhou, China. *Environ. Pollut.* **2017**, *223*, 295–304. [[CrossRef](#)] [[PubMed](#)]
55. Zheng, H.; Kong, S.; Xing, X.; Mao, Y.; Hu, T.; Ding, Y.; Li, G.; Liu, D.; Li, S.; Qi, S. Monitoring of volatile organic compounds (VOCs) from an oil and gas station in northwest China for 1 year. *Atmos. Chem. Phys.* **2018**, *18*, 4567–4595. [[CrossRef](#)]
56. Zhan, J.; Feng, Z.; Liu, P.; He, X.; He, Z.; Chen, T.; Wang, Y.; He, H.; Mu, Y.; Liu, Y. Ozone and SOA formation potential based on photochemical loss of VOCs during the Beijing summer. *Environ. Pollut.* **2021**, *285*, 117444. [[CrossRef](#)] [[PubMed](#)]